札幌医学雑誌　89（1 － 6）31 ～ 40（2021）　doi：10.15114 / smj.89.31

ORIGINAL

Enhancement of Dormant Pathways in the Brain following Rat Contusive Spinal Cord Injury

Ryosuke HIROTA[1, 2], Masanori SASAKI[1], Toshihiko YAMASHITA[2], Osamu HONMOU[1]

[1] Department of Neural Regenerative Medicine, Research Institute for Frontier Medicine, Sapporo Medical University School of Medicine

[2] Department of Orthopaedic Surgery, Sapporo Medical University School of Medicine

ABSTRACT

Background:

Spinal cord injury (SCI) induces distal effects on neural activity in the brain. To date, precise, high quality anatomical studies have not been performed. The goal of this study was to delineate neuroanatomical enhancement of dormant pathways in the brain following SCI using an appropriate serotype of an adeno-associated-virus (AAV) with a CAG promotor.

Methods:

We injected three serotypes of an AAV viral vector with a CAG promoter and a green fluorescent protein (GFP) tag, AAV-2, -5, and -8-CAG-GFP, unilaterally, into one hemisphere of the rat brain to compare the utility of the three serotypes as neural tracers. Then, fluorescent labeling and confocal microscopy were used to assess changes in neural pathways for an optimal serotype in intact and SCI rats.

Results:

The AAV-8 serotype provided the optimal tracing of neural pathways in the brain in terms of transduction properties, migratory capabilities and cell labeling specificity. Enhanced both interhemispheric and inter-nucleus connections were observed six weeks after SCI induction using the AAV-8-CAG-GFP viral tracer.

Conclusions:

AAV serotype 8 with a CAG promotor was the most useful neural AAV tracer for elucidating changes in neural pathways in the brain. SCI-induced enhancement of brain network was detectable with the AAV-8-CAG-GFP viral tracer in our model system.

(Accepted January 8, 2020)

Key words: adeno-associated virus, spinal cord injury, neural pathways

1 Introduction

Recent spinal cord injury (SCI) studies have shown that the brain undergoes regenerative reactions following SCI[1-3], in addition to the local regenerative responses that occur within the injured spinal cord[4, 5]. Non anatomical studies such as metabolic or neural activities in the brain after SCI have reported that dynamic compensation occurs in the brain that suggests network reorganization; these compensatory mechanisms could contribute to functional improvement after SCI[6-8]. In the brain imaging study using positron emission tomography, increased activation of bilateral cortex and contralateral ventral striatum were observed during recovery from cervical SCI lesion in the nonhuman primate[9]. Additionally, a resting-state functional Magnetic Resonance Imaging (MRI) study of SCI patients also demonstrated functional network plasticity in the brain as a result of injury to the spinal cord[8]; however, to date, precise, high quality anatomical studies have not been performed. Thus, visualizing the structural reorganization of neural pathways in

the brain following SCI using neuroanatomical techniques may be crucial for providing mechanistic insights at a cellular level.

To delineate neural pathways in the central nervous system, neural tracers are widely used. As a result of recent advances in viral tracing technology, numerous viral tracers have been tested; of them, the adeno-associated virus (AAV) has distinct properties that allow it to transduce target neurons with gene sequences coding for fluorescent marker proteins such as green fluorescent protein (GFP) or tdTomato, with no apparent cytotoxicity[10]. In AAVs infected neurons, these fluorescent proteins accumulate throughout the cytoplasm of the cell, including the cell body, dendrites, axon, and axon terminals, providing precise fluorescent labeling of neural pathways[11]. Because AAVs vectors produce robust florescent signal following infection, therefore, conventional confocal microscopy or light-sheet microscopy can detect these signals directly without multiple histological staining steps[12]. AAVs provide advantages that increase overall methodological flexibility in addition to their sensitivity, specificity, and reliability as anterograde tracers to delineate neural connections compared to conventional tracers such as horseradish peroxidase (HRP), *Phaseolus vulgaris* leucoagglutinin (PHA-L), and biotinylated dextran amine (BDA) in rodent brain[12]. Thus, AAVs could be a powerful tool to trace neural pathways to improve our understanding of the reorganization that occurs in the brain following SCI.

In the current study, we compared fluorescent intensities following transduction with three serotypes, AAV-2[11, 13], AAV-5[13, 14] and AAV-8[15], to evaluate the ability to provide optimal neural tracing in intact brains. Because several serotypes have been reported that each has own properties in terms of cell type selectivity (AAV tropism)[10, 16], it was important to select an appropriate serotype to study neural pathways in our model system. The AAV-2, -5 and -8-CAG-GFP viral tracers were injected into the brain; among these serotypes, AAV-8 provided the optimal ability to trace neural pathways in brain in our study. Then, we tested the hypothesis that the enhancement of dormant pathways induced by SCI could be detected with our AAV-8-CAG-GFP viral tracer.

2 Materials and Methods

Animals

All experiments were conducted in accordance with the institutional guidelines of Sapporo Medical University. The use of animals in this study was approved by the Animal Care and Use Committee and the Committee for Security of Recombinant DNA Experiments of Sapporo Medical University.

Viral tracer injections

GFP-encoding AAVs with a CAG promoter and tdTomato-encoding AAVs with a CAG promoter (AAV-2, -5 and -8-CAG-GFP/tdTomato) were purchased from Vector Biolabs (Philadelphia, PA, USA). Adult (7-week old) male Sprague-Dawley (SD) rats (250-300g) were placed on a stereotaxic frame under ketamine (75 mg/kg, intraperitoneal) and xylazine (10 mg/kg, intraperitoneal) anesthesia. A craniotomy was performed to expose the sensorimotor cortex. GFP-encoding AAVs were injected into the right hemisphere. Six injections for cortex (AAVs; 4.0×10^{10} genome copy/μl, 0.5 μl per site) were performed at the following coordinates: 1.0 mm lateral; 1.5 mm, 1.0 mm depth, and -1.0 mm, 0 mm, 1.0 mm posterior to bregma using a nanoliter-injector (World Precision Instrument Inc., Sarasota, FL, USA) attached to a pulled glass pipette[17]. The method used in this study allows us to perform precise micro-delivery of viral vectors to the localized region in the brain. The needle was left in place for 3 min before moving to the next site. tdTomato-encoding AAVs were also injected into the left hemisphere. One point injection for brain stem (AAVs; 4.0×10^{10} genome copy/μl, 0.21 μl) was performed at the following coordinates: 1.0 mm lateral; 8.0 mm depth, and 6.0 mm, posterior to bregma.

Histological analysis

Six weeks after tracer injections[18], rats were perfused transcardially with cold phosphate-buffered saline (PBS) followed by 4% paraformaldehyde under deep anesthesia with an intraperitoneal injection of ketamine (75 mg/kg) and xylazine (10 mg/kg). Whole brains were dissected out and were stored at - 80 °C until use. Coronal sections were cut to 50 μm thickness using a cryostat (Sakura Seiki Co, Tokyo, Japan).

One section per animal was selected and cut according to the rat stereotaxic atlas[19]. We cut the frozen sections as follows: to compare AAVs transduction properties, sections were cut at Bregma -2 mm (Fig. 1D, 1E); to measure and compare anterograde migratory capability, sections were cut at Bregma -2 mm (Fig. 1F) and Bregma -8 mm (2D, 2E); to test the specificity of cell labeling, sections were cut at Bregma 0 mm (Fig. 3); to assess alterations in interhemispheric connectivity following SCI, sections were cut at Bregma 0 mm (Fig. 5); to assess alterations in neural connectivity within the brain stem following SCI, sections were cut at Bregma -6 mm (Fig6). Then, these sections were washed in PBS- 0.1% Tween 20 (PBS-T) 3 times.

The sections were examined using a confocal microscopy (Zeiss LSM780 ELYRA S.1 system). Sections were viewed directly to assess GFP and tdTomato fluorescence. Intensities of GFP or tdTomato signals were quantified using ImageJ software bundled with Java 1.8.0_172 (National Institutes of Health, Bethesda MD, USA, http://rsv.info.nih.gov/ij/)[11, 17, 20].

SCI model

Contusive SCI was performed as described previously[21]. Briefly, adult (7-week old) male SD rats (250-300g) were anesthetized with an intraperitoneal injection of ketamine (90 mg/kg, intraperitoneal) and xylazine (4 mg/kg, intraperitoneal). After skin incision, the T9 vertebra was stabilized, a laminectomy was performed at the T9-10 level of the spinal cord, and a 150 kdyn contusion was delivered to the spinal cord using an Infinite Horizons impactor (Precision Systems and Instrumentation, LLC, Lexington, KY, USA). Appropriate post-operative care was provided for all animals, including twice-daily manual bladder expression for up to 14 days. Rats were housed in an atmosphere of 50% humidity at a temperature of 24 ± 2°C. At day 14 after SCI induction, AAV-8-CAG-GFP virus were injected to the both SCI animals and age-matched intact animals[22-27] as described above.

Behavioral testing

Open field locomotor function was assessed using the Basso, Beattie, and Bresnahan (BBB) locomotor rating scale[28]. Intact and SCI rats were scored 2 days prior to SCI induction, and at 2 days intervals thereafter until sacrifice at 26 days post-SCI induction (n = 8/Intact group, n = 8/SCI group).

Statistics

All statistical analyses were performed with Statistical Package for the Social Sciences (SPSS) 21 for Macintosh (IBM, Inc, IL, USA). Groups were compared by one-way ANOVA, and the Tukey-Kramer test was used for *post-hoc* comparisons. Comparisons between two groups were performed using the student *t*-test. Data were expressed as the mean ± standard error of the mean (SEM). Differences were considered statistically significant at $p < 0.05$.

3 Results

3.1 *Transduction properties at the site of injection did not differ among the three AAV serotypes*

To compare the transduction properties of the AAV-2, -5 and -8 serotypes at the injection site in the brain, GFP-encoding AAVs with a CAG promoter (AAV-2, -5 and -8-CAG-GFP) were injected into left hemisphere. Six weeks after injection of the AAVs, we examined fluorescent intensity of these serotypes in the coronal brain sections (Fig.1). Intense GFP+ fluorescence was observed in the left hemisphere of the brain around the injection site under a confocal microscopy.

Quantification of GFP fluorescent signal intensities across the whole section (Fig. 1D: AAV-2: 27.0 ± 6.3, n=4; AAV-5: 36.1 ± 8.8, n=4; AAV-8: 37.2 ± 9.0, n=4) and around the injection site (Fig. 1A1, 1B1, 1C1) (Fig. 1E: AAV-2: 359.6 ± 70.7, n=4; AAV-5: 347.9 ± 68.1, n=4; AAV-8: 375.3 ± 70.4, n=4) revealed that there were no significant differences among the three AAV serotypes around the injection sites.

3.2 *AAV Serotype 8 with a CAG promotor exhibited the highest anterograde migratory capability in the intact brain*

To measure anterograde migratory capability, we assessed fluorescent signal intensities of coronal sections from the left internal capsule (Fig. 1F: AAV-2: 181.9 ± 36.5, n=4; AAV-5: 176.5 ± 33.8, n=4; AAV-8: 185.4 ± 39.9, n=4) and the cerebral peduncle in the brain stem (Fig. 2). Quantifications of GFP fluorescent intensities revealed that the

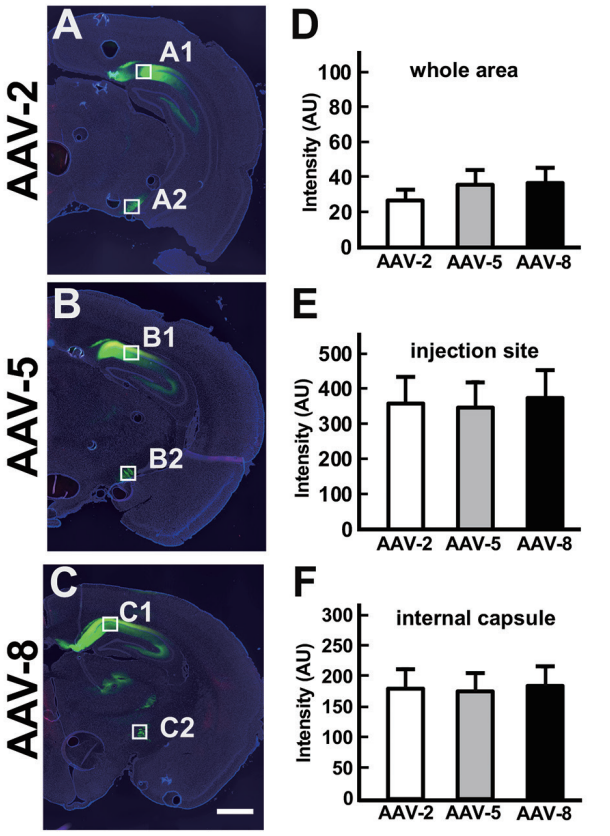

Figure 1. Coronal brain sections (Bregma -2 mm) injected with (A) AAV-2, (B) AAV-5, (C) AAV-8-CAG-GFP viral vectors. The boxed area in A1, B1, C1 indicates labeling around the injection sites, and the boxed area in A2, B2, C2 indicates labeling in the internal capsule for the three serotypes, respectively. Quantification of signal intensity across the whole section (D) around the injection site (E) and in the internal capsule (F). Scale bar = 2 mm.

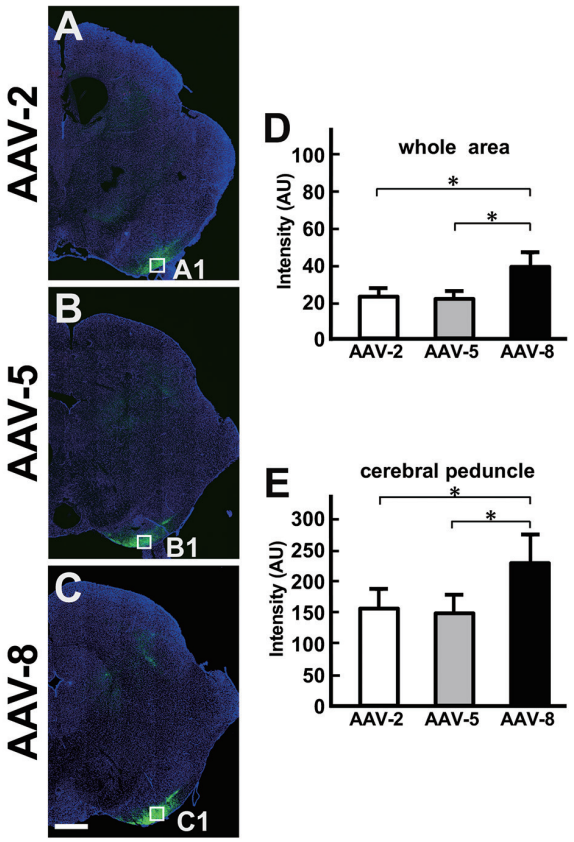

Figure 2. Coronal brain sections (Bregma -8 mm) injected with (A) AAV-2, (B) AAV-5, (C) AAV-8-CAG-GFP. The boxed area in A1, B1, C1 are regions of interest showing labeling in the cerebral peduncle for the three serotypes, respectively. Quantification of signal intensity across the whole section (D) and in the cerebral peduncle (E). Scale bar = 1mm. * $p<0.05$.

signal intensity of fluorescent labeling of the GFP-tagged AAV-8 was higher than for AAV-2 or AAV-5 in the whole area including the cerebral peduncle (Fig. 2D: AAV-2: 22.5 ± 3.1, n=4; AAV-5: 21.3 ± 3.0, n=4; AAV-8: 38.8 ± 5.3, n=4; $p < 0.05$) and in the cerebral peduncle alone (Fig. 2A1. 2B1, 2C1, Fig. 2E: AAV-2: 156.2 ± 30.5, n=4; AAV-5: 148.6 ± 29.3, n=4; AAV-8: 229.3 ± 44.6, n=4; $p < 0.05$), though no statistical differences in fluorescent labeling were observed in the internal capsule (Fig. 1A2, 1B2, 1C2). These results show that the anterograde migratory capability of serotype 8 of AAV with CAG promotor was the highest in this study.

3.3 *AAV serotype 8 with a CAG promotor resulted in the highly specific cell labeling in the intact brain*

To test the specificity of cell labeling, AAV-8-CAG-GFP virus was injected into the right cortex and td AAV-8-CAG-tdTomato was injected into the left cortex (Fig. 3A, n=4). Six weeks later, we examined fluorescent intensity in the coronal brain sections under a confocal microscope (Fig. 3B). GFP^+ fluorescent signals (green) were observed in the left cortex (Fig. 3C in Fig. 3B box), throughout the corpus callosum, as well as in the area around the injection site in the right cortex. High power imaging revealed that numerous GFP^+ neural fibers and cells were clearly visible in the left cortex (Fig. 3C). Fluorescent tdTomato signals (red) were also observed in the left cortex where they were injected; high power imaging revealed tdTomato+ fibers and cells (Fig. 3D in Fig. 3B box). These cells were not co-labeled in the left cortex (Fig. 3E). Thus, the AAV-8 serotype with a CAG promotor used in this study resulted in cell-specific labeling.

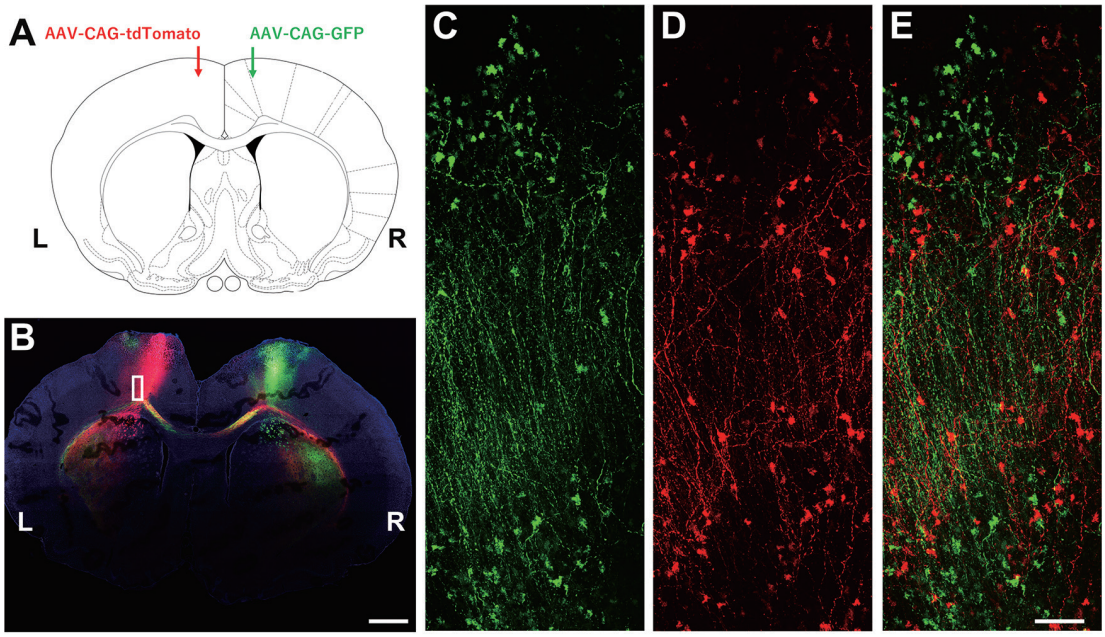

Figure 3. Schematic drawing of injection sites for AAV-8-CAG-GFP and AAV-8-CAG-tdTomato (A). Low power confocal microscopic tiled image (B). C, D and E are region of interest identified by the boxed area in B. Scale bars = 2 mm (B), 100 μm (C, D, E).

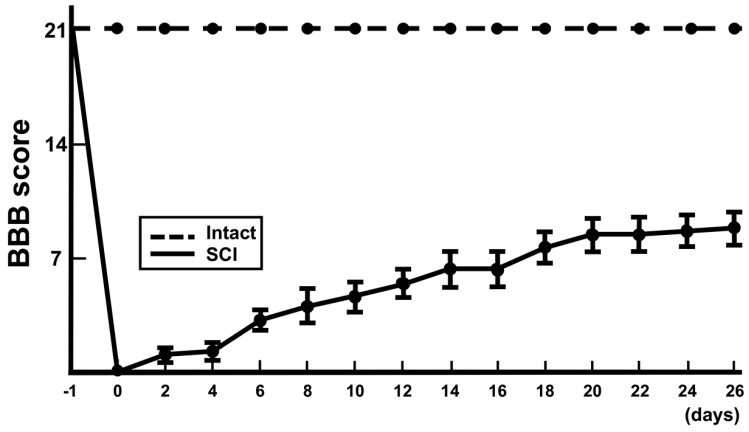

Figure 4. Behavioral analysis of locomotor function with BBB score.

3.4 *Endogenous recovery of locomotor function following SCI*

To confirm that our animal model of SCI showed endogenous improvement of locomotor function following injury, open field locomotor activity was assessed using the BBB scoring scale at two-day intervals from SCI until 26 days post-SCI. Before SCI induction, BBB scores had a value of 21. SCI animals demonstrated near-complete hind limb paraplegia immediately after SCI, but exhibited a gradual improvement that plateaued 20 days after SCI (BBB score; 8.6 ± 1.24, n=8) (Fig. 4). The BBB scores of intact rats (n=8) remained 21 for study period. This is consistent with our previous studies[21, 29, 30] and we used this model system in the current study.

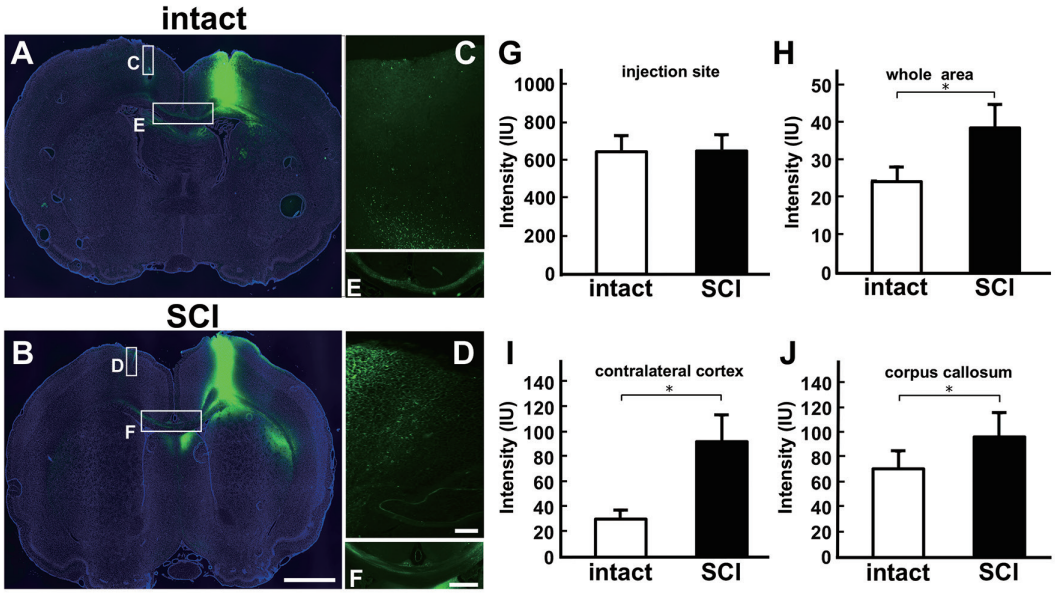

Figure 5. Coronal brain sections (Bregma 0 mm) injected with AAV-8-CAG-GFP from intact (A) and SCI (B) animals. The boxed areas in A are C, E, and boxed areas in B are D, F, respectively. Quantification of signal intensity around the injection site (G), across the whole section (H), in the contralateral cortex (I), and at the corpus callosum (J). Scale bars = 2 mm (A, B), 100 μm (C, D), 300 μm (E, F). * $p<0.05$, ** $p<0.01$.

3.5 *SCI induced enhanced interhemispheric connectivity detectable with the AAV-8-CAG-GFP vector*

To detect the enhanced interhemispheric connections following SCI, we injected an AAV-8-CAG-GFP vector in the left motor cortex of intact (Fig. 5A) and SCI (Fig. 5B) animals. The fluorescent intensity at the injection sites was similar in both intact (Fig. 5A) and SCI (Fig. 5B) animals; however, the intensities across whole section (Fig. 5B), in the contralateral cortex (Fig. 5D), and at the corpus callosum (Fig. 5F) in the SCI animals were greater than in whole section (Fig. 5A), contralateral cortex (Fig. 5C), and corpus callosum (Fig. 5E) of the intact animals.

Quantitative analysis demonstrated that fluorescent signal intensities in the SCI animals were higher than in the intact animals in the whole area (Fig. 5H: intact: 24.5 ± 4.7, n=4; SCI: 38.8 ± 6.3, n=4; $p < 0.05$), the contralateral cortex (Fig. 5I: intact: 31.1 ± 6.9, n=4; SCI: 93.2 ± 20.3, n=4; $p < 0.01$), and the corpus callosum (Fig. 5J: intact: 71.6 ± 15.4, n=4; SCI: 97.3 ± 18.9, n=4; $p < 0.05$), though fluorescence around the injection sites in the cortex did not differ (Fig. 5G: intact: 646.4 ± 80.3, n=4; SCI: 650.5 ± 79.4, n=4). These results show that the enhanced interhemispheric connectivity induced by SCI could be detected with the use of AAV-8-CAG-GFP viral tracer.

3.6 *SCI induced enhanced inter-nucleus connections within the brain stem detected with AAV-8-CAG-GFP vector*

To detect the enhanced inter-nucleus connections within brain stem following SCI, we injected an AAV-8-CAG-GFP vector around the left substantial nigra (SN) in both intact and SCI animals (Fig. 6A). The intensity at the injection sites was similar in both intact (Fig. 6B) and SCI (Fig. 6C) animals; however, the GFP fluorescent intensities across whole sections (Fig. 6C), in the transverse fiber of the pons (Fig. 6E), and in the contralateral subthalamic nucleus (STN) (Fig. 6G) in the SCI animals were greater than in the same areas of intact animals (Fig. 6B, Fig. 6D, and Fig. 6F, respectively.)

Quantitative analysis demonstrated that the fluorescent signal intensities of SCI animals were higher than those of intact animals in the whole area (Fig. 6I: intact: 56.7 ± 9.5, n=4; SCI: 91.4 ± 15.2, n=4; $p < 0.05$), in the transverse fibers of the pons (Fig. 6J: intact: 88.5 ± 24.4, n=4; SCI: 144.1 ± 40.9, n=4; $p < 0.05$), and in the contralateral STN (Fig. 6K: intact: 190.6 ± 38.0, n=4; SCI: 350.1 ± 66.4, n=4; $p < 0.05$), though fluorescent intensities

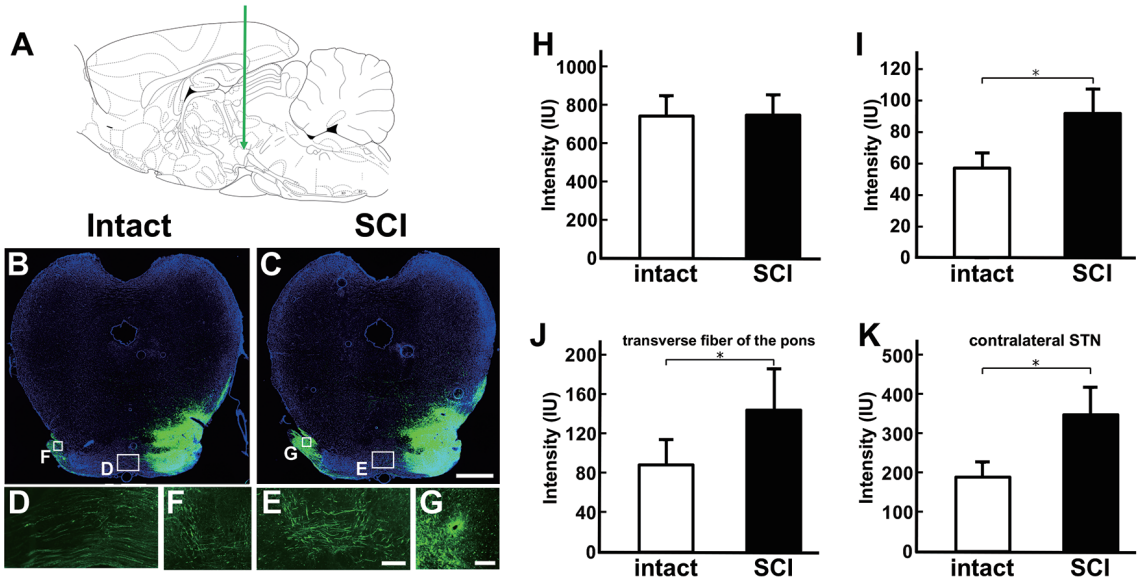

Figure 6. Schematic drawing of injection sites (green arrow) of AAV-8-CAG-GFP (A). Coronal brain sections (Bregma -6 mm) injected with AAV-8-CAG-GFP virus in intact (B) and SCI (C) animals. The boxed areas in B are D (transverse fiber of the pons) and F (contralateral STN). Boxed area in C are E (transverse fiber of the pons) and G (contralateral STN), for intact and SCI animals, respectively. Quantification of signal intensity around the injection site (H), across the whole section (I) in the transverse fiber of the pons (J) and in the contralateral STN (K). Scale bars = 1 mm (B, C), 250 μm (D, E), and 100 μm (F, G). * $p<0.05$.

around the injection site in the SN did not differ (Fig. 6H: intact: 745.3 ± 103.4, n=4; SCI: 750.1 ± 107.2, n=4). These results indicate that there was enhanced inter-nucleus connections within brain stem induced by SCI, especially in ipsilateral SN to contralateral STN connections, which were detectable using the AAV-8-CAG-GFP viral vector.

4 Discussion

In this study, we demonstrated that serotype 8 was the most useful for neuronal tracing in the brain. First, in terms of transduction properties, GFP^+ fluorescent signals were observed at the injection sites for all three AAV serotypes used in the current study. These signals were localized around the injection sites and did not spread to other areas of the brain. These observations are consistent with those of other studies that have investigated the potential of AAV vectors for neural tracing in the brain[17, 31].

Second, in terms of anterograde migratory capability, AAV-8 displayed distinct properties for tracing neural pathways in the brain. Following microinjection of the AAV-8-CAG-GFP viral vector, we observed migration from the cortex to the brain stem. Although we did not find differences between the three AAVs at the level of the internal capsule, we did observe higher florescent signals at the cerebral peduncle following AAV-8-CAG-GFP viral vector injection; this observation indicates that AAV-8 has greater migratory capabilities compared to AAV-2 and AAV-5.

Third, we observed interhemispheric projections across the corpus callosum to confirm the specificity of cell labeling of the AAV serotype 8 neural tracer with both AAV8-CAG-GFP and AAV-8-CAG-tdTomato viral vectors and confocal microscopy. Injection sites in both hemispheres showed similarly intense fluorescent signals, and high-power confocal imaging revealed that projection fibers with GFP^+ fluorescence could be clearly detected in the opposite cortex through the corpus callosum. GFP^+ cells and fibers were not co-localized with $tdTomato^+$ cells and fibers; this cellular specificity is another unique property of AAV-8-CAG-GFP and AAV-8-CAG-tdTomato viral vectors in rodent. Thus, AAV-8 with a CAG promotor used in this study resulted in specific cell labeling. Taken together, AAV-8 could be the most useful serotype for tracing changes in neural pathways following SCI compared to the AAV-2 and AAV-5 serotypes used in this study.

Enhanced neural pathways was detected following AAV-8-CAG-GFP viral vector injection, both in terms of interhemispheric and inter-nucleus connections in this contusive SCI rat model, which we confirmed endogenous functional recovery evaluated with BBB scoring in the open field test in this study. While previous studies reported that interhemispheric networks are poorly detectable in healthy human subjects through MRI diffusion tensor imaging[33], and also inter-nucleus connection (the SN to contralateral STN connection) within the brain stem are shown using intact rats[34]. However, these dormant pathways were significantly enhanced in SCI animals in this study. The precise role of these pathways following the SCI are not known; it has been reported, however, that brain network reorganization occurs during recovery from SCI to enhance activation of dormant connectivity[6, 35]. Thus, the changes we observed in brain regions following SCI observed in the current study could be partially associated with the mechanisms promoting endogenous recovery, though these enhancements in neural connectivity alone might not be sufficient to provide full recovery.

In the current study, we employed methods of both precise delivery of AAV-8-CAG-GFP/tdTomato viral vectors to the localized region and sophisticated computerized quantitative analysis using a software with high quality microscopic images. Combination of these methods is widely used to demonstrate quantitative analysis of neural traceability.

In summary, we have shown that AAV-8-CAG-GFP/tdTomato viral vectors are the most useful neural tracers for visualizing the reorganization of neural connections in the brain following SCI. Future studies with application of both AAV-8-CAG-GFP/tdTomato viral vectors and this consistent SCI model system will provide valuable data for elucidating potential cellular mechanisms associated with improved functional outcomes following potential therapeutic interventions.

Acknowledgments

This work was supported in part by JSPS KAKENHI grant numbers 18K09072 (to R.H.), 16K10794 (to M.S.).

Conflict of interest

There is no competing financial interest.

References

1. Thompson K, DiBona V, Dubey A, Crockett D, Rasin M-R. Acute adaptive responses of central sensorimotor neurons after spinal cord injury. Transl Neurosci 2010; 1: 268-278.
2. Endo T, Spenger C, Tominaga T, Brené S, Olson L. Cortical sensory map rearrangement after spinal cord injury: fMRI responses linked to Nogo signalling. Brain 2007; 130: 2951-2961.
3. Aguilar J, Humanes-Valera D, Alonso-Calvino E, Yague JG, Moxon KA, Oliviero A, Foffani G. Spinal cord injury immediately changes the state of the brain. J Neurosci 2010; 30: 7528-7537.
4. Fawcett JW. Overcoming inhibition in the damaged spinal cord. J Neurotrauma. 2006; 23: 371-383.
5. Siddiqui AM, Khazaei M, Fehlings MG. Translating mechanisms of neuroprotection, regeneration, and repair to treatment of spinal cord injury. Prog Brain Res 2015; 218: 15-54.
6. Isa T. The Brain Is Needed to Cure Spinal Cord Injury. Trends Neurosci 2017; 40: 625-636.
7. Nishimura Y, Onoe H, Morichika Y, Perfiliev S, Tsukada H, Isa T. Time-dependent central compensatory mechanisms of finger dexterity after spinal cord injury. Science 2007; 318: 1150-1155.
8. Hawasli AH, Rutlin J, Roland JL, Murphy RKJ, Song S-K, Leuthardt EC, Shimony JS, Ray WZ. Spinal Cord Injury Disrupts Resting-State Networks in the Human Brain. J Neurotrauma 2017; 35: 864-873.
9. Isa T, Nishimura Y. Plasticity for recovery after partial spinal cord injury - hierarchical organization. Neurosci Res 2014; 78: 3-8.
10. Betley JN, Sternson SM. Adeno-associated viral vectors for mapping, monitoring, and manipulating neural circuits. Hum Gene Ther 2011; 22: 669-677.
11. Soderblom C, Lee DH, Dawood A, Carballosa M, Jimena Santamaria A, Benavides FD, Jergova S, Grumbles RM, Thomas CK, Park KK, Guest JD, Lemmon VP, Lee JK, Tsoulfas P. 3D Imaging of Axons in Transparent Spinal Cords from Rodents and Nonhuman Primates. eNeuro doi: 10.1523/ENEURO.0001-15.2015.
12. Wang Q, Henry AM, Harris JA, Oh SW, Joines KM, Nyhus J, Hirokawa KE, Dee N, Mortrud M, Parry S, Ouellette B, Caldejon S, Bernard A, Jones AR, Zeng H, Hohmann JG. Systematic comparison of adeno-associated virus and biotinylated dextran amine reveals equivalent sensitivity between tracers and novel projection targets in the mouse brain. J Comp Neurol 2014; 522: 1989-2012.
13. Liu Y, Keefe K, Tang X, Lin S, Smith GM. Use of self-complementary adeno-associated virus serotype 2 as a tracer for labeling axons: implications for axon regeneration. PLoS One. 2014; 9(2): e87447. Epub

2014/02/06. doi: 10.1371/journal.pone.0087447.
14. Asboth L, Friedli L, Beauparlant J, Martinez-Gonzalez C, Anil S, Rey E, et al. Cortico-reticulo-spinal circuit reorganization enables functional recovery after severe spinal cord contusion. Nat Neurosci. 2018; 2: 576-588.
15. Favuzzi E, Marques-Smith A, Deogracias R, Winterflood CM, Sanchez-Aguilera A, Mantoan L, et al. Activity-Dependent Gating of Parvalbumin Interneuron Function by the Perineuronal Net Protein Brevican. Neuron. 2017; 95: 639-655.
16. Nathanson JL, Yanagawa Y, Obata K, Callaway EM. Preferential labeling of inhibitory and excitatory cortical neurons by endogenous tropism of adeno-associated virus and lentivirus vectors. Neuroscience 2009; 161: 441-450.
17. Nagahama H, Nakazaki M, Sasaki M, Kataoka-Sasaki Y, Namioka T, Namioka A, Oka S, Onodera R, Suzuki J, Sasaki Y, Kocsis JD, Honmou O. Preservation of interhemispheric cortical connections through corpus callosum following intravenous infusion of mesenchymal stem cells in a rat model of cerebral infarction. Brain Res 2018; 1695: 37-44.
18. Ueno M, Nakamura Y, Li J, Gu Z, Niehaus J, Maezawa M, et al. Corticospinal Circuits from the Sensory and Motor Cortices Differentially Regulate Skilled Movements through Distinct Spinal Interneurons. Cell Rep 2018; 23: 1286-1300.e7
19. Paxinos G, Watson C. The Rat Brain in Stereotaxic Coordinates. 123 Library. 6 ed: Academic Press; 2007.
20. Tanguy Y, Biferi MG, Besse A, Astord S, Cohen-Tannoudji M, Marais T, Barkats M. Systemic AAVrh10 provides higher transgene expression than AAV9 in the brain and the spinal cord of neonatal mice. Front Mol Neurosci 2015; 8: 36. doi: 10.3389/fnmol.2015.00036
21. Oshigiri T, Sasaki T, Sasaki M, Kataoka-Sasaki Y, Nakazaki M, Oka S, Morita T, Hirota R, Yoshimoto M, Yamashita T, Hashimoto-Torii K, Honmou O. Intravenous Infusion of Mesenchymal Stem Cells Alters Motor Cortex Gene Expression in a Rat Model of Acute Spinal Cord Injury. J Neurotrauma 2019; 36: 411-420.
22. Bezdudnaya T, Marchenko V, Zholudeva LV, Spruance VM, Lane MA. Supraspinal respiratory plasticity following acute cervical spinal cord injury. Exp Neurol. 2017; 293: 181-189.
23. Brakel K, Aceves AR, Aceves M, Hierholzer A, Nguyen QN, Hook MA. Depression-like behavior corresponds with cardiac changes in a rodent model of spinal cord injury. Exp Neurol. 2019; 320: 112969. doi: 10.1016/j.expneurol.2019.112969.
24. Xu Y, Kitada M, Yamaguchi M, Dezawa M, Ide C. Increase in bFGF-responsive neural progenitor population following contusion injury of the adult rodent spinal cord. Neurosci Lett. 2006; 397: 174-179.
25. Goulao M, Ghosh B, Urban MW, Sahu M, Mercogliano C, Charsar BA, et al. Astrocyte progenitor transplantation promotes regeneration of bulbospinal respiratory axons, recovery of diaphragm function, and a reduced macrophage response following cervical spinal cord injury. Glia. 2019; 67: 452-466.
26. Povysheva TV, Mukhamedshina YO, Rizvanov AA, Chelyshev YA. PTEN expression in astrocytic processes after spinal cord injury. Mol Cell Neurosci. 2018; 88: 231-239.
27. Patar A, Dockery P, Howard L, McMahon SS. Cell viability in three ex vivo rat models of spinal cord injury. J Anat. 2019; 234: 244-251.
28. Basso DM, Beattie MS, Bresnahan JC. A sensitive and reliable locomotor rating scale for open field testing in rats. J Neurotrauma. 1995; 12: 1-21.
29. Morita T, Sasaki M, Kataoka-Sasaki Y, Nakazaki M, Nagahama H, Oka S, Oshigiri T, Takebayashi T, Yamashita T, Kocsis JD, Honmou O. Intravenous infusion of mesenchymal stem cells promotes functional recovery in a model of chronic spinal cord injury. Neuroscience 2016; 335: 221-231.
30. Matsushita T, Lankford KL, Arroyo EJ, Sasaki M, Neyazi M, Radtke C, Kocsis JD. Diffuse and persistent blood-spinal cord barrier disruption after contusive spinal cord injury rapidly recovers following intravenous infusion of bone marrow mesenchymal stem cells. Exp Neurol 2015; 267: 152-164.
31. Watakabe A, Ohtsuka M, Kinoshita M, Takaji M, Isa K, Mizukami H, Ozawa K, Isa T, Yamamori T. Comparative analyses of adeno-associated viral vector serotypes 1, 2, 5, 8 and 9 in marmoset, mouse and macaque cerebral cortex. Neurosci Res 2015; 93: 144-157.
32. Zingg B, Chou XL, Zhang ZG, Mesik L, Liang F, Tao HW, Zhang LI. AAV-Mediated Anterograde Transsynaptic Tagging: Mapping Corticocollicular Input-Defined Neural Pathways for Defense Behaviors. Neuron 2017; 93: 33-47.
33. Liu J, Qin W, Zhang J, Zhang X, Yu C. Enhanced interhemispheric functional connectivity compensates for anatomical connection damages in subcortical stroke. Stroke 2015; 46: 1045-1051.
34. Marani E. LNE, Heida T., Usunoff K.G., Nigro-subthalamic and nigro-trigeminal projections in the rat. In: Bamidis P.D. Pallikarakis N. editor. XII Mediterranean Conference on Medical and Biological Engineering and Computing 2010: May 27-30, 2010, Chalkidiki, Greece. [Berlin]: Springer, c2010
35. Wang W, Tang S, Li C, Chen J, Li H, Su Y, Ning B. Specific Brain Morphometric Changes in Spinal Cord Injury: A Voxel-Based Meta-Analysis of White and Gray Matter Volume. J Neurotrauma 2019; 36: 2348-2357.

別刷請求先：廣田　亮介
〒060-8556　札幌市中央区南1条西17丁目
札幌医科大学医学部　整形外科学講座
TEL：011-611-2111（内線33330）
FAX：011-641-6026

脊髄損傷後の脳における神経連絡の賦活化

廣田亮介[1,2)]，佐々木祐典[1)]，山下敏彦[2)]，本望　修[1)]

[1)] 札幌医科大学医学部附属フロンティア医学研究所　神経再生医療学部門
[2)] 札幌医科大学医学部整形外科学講座

【背景】

これまでに脊髄損傷後に生じる脳内の神経経路の再構築が，Positron Emission Tomography や MRI diffusion tensor imaging などを用いて報告されているが，詳細な神経解剖学的手法を用いた報告は少ない．本研究の目的は順行性神経トレーサーとして知られるアデノ随伴ウイルス（AAV）を用いて，脊髄損傷後の脳内における神経回路の変化を詳細に解析することである．

【方法】

第 1 に，正常ラット（SD，250-300g）を用いて，CAG プロモーターを搭載した GFP 発現 AAV ベクター（2 型・5 型・8 型）をそれぞれ片側大脳半球に局所注入し，GFP の蛍光輝度を定量することで AAV の脳内における形質導入効率，順行性追跡能，細胞選択的標識能が高い血清型を確認した．第2に，IHインパクターを用いて脊髄損傷モデルラットを作成し，適切な AAV ベクターを大脳皮質および黒質周囲に局所注入し，脊髄損傷後に生じる脳内の神経経路の変化を解析した．

【結果】

① 3 種の血清型では，局所注入部位において，各血清型での GFP の蛍光輝度に有意差を認めず，形質導入効率には差が無かった．
② 一方，GFP の蛍光輝度は，内包では各血清型での GFP の蛍光輝度に有意差を認められなかったが，大脳脚では 8 型 (AAV-8-CAG-GFP) を局所注入した群で有意に強い GFP の蛍光輝度を認めたことから，順行性追跡能は 8 型が最も高いことがわかった．
③ AAV-8-CAG-GFP を右大脳皮質に局所注入した結果，AAV-8-CAG-GFP は脳梁を介して，左側の大脳皮質にまで到達し，GFP 陽性の神経線維を確認することが出来た．また，AAV-8-CAG-tdTomato を左大脳皮質に局所注入した結果，局所において tdTomato が形質導入された神経細胞や線維と，GFP 陽性の神経細胞や線維は共存しておらず，AAV-8-CAG ベクターの高い細胞選択的標識能を確認した．
④ 脊髄損傷モデルを作成した後に，AAV-8-CAG-GFP を右大脳皮質に局所注入した結果，脳梁を介した左側皮質への神経経路が賦活化されていた．
⑤ 脊髄損傷モデルを作成した後に，AAV-8-CAG-GFP を右黒質周囲に局所注入した結果，右黒質－左視床下核間の神経経路が賦活化されていた．

【結論】

CAG プロモーターを搭載した AAV-8 は，脳内における形質導入効率，順行性追跡能，細胞選択的標識能が高いことが判明した．さらに，同ベクターを用いて，脊髄損傷後の脳を解析した結果，神経回路の賦活化が生じていることが示唆された。